applied sciences

MDPI

*Article*

# Research on Mechanical Properties and Damage Constitutive Model of Water-Bearing Coal

**Feng Ju [1,2], Dong Wang [2,*], Zhongwei Wang [3], Meng Xiao [1,2], Zequan He [1,2], Pai Ning [1,2], Tengfei Wang [1,2], Cheng Zhou [2], Yazhen Zhang [2], Li Li [2] and Chaosen Yan [2]**

[1] State Key Laboratory for Geomechanics and Deep Underground Engineering, China University of Mining and Technology, Xuzhou 221116, China
[2] School of Mechanics and Civil Engineering, China University of Mining and Technology, Xuzhou 221116, China
[3] Taiyuan Research Institute, China Coal Technology and Engineering Group, Taiyuan 030006, China
* Correspondence: mechanics@cumt.edu.cn; Tel.: +86-182-6263-9816

**Featured Application: The research conclusions of this paper can provide a reference for the analysis, design, and construction of water-related engineering in coal mines.**

**Abstract:** Many water-related problems are confronted in coal mining, and the mechanical properties of coal inevitably deteriorate due to water–rock interactions. Therefore, it is necessary to study the macroscopic mechanical properties and damage constitutive model of water-bearing coal for safe mining. The uniaxial compression tests of raw coal samples with five moisture contents under four loading rates were carried out. Based on the test, the Drucker–Prager criterion is introduced to describe the failure law of micro-elements; assuming that the strength of micro-elements obeys a two-parameter Weibull distribution, a three-stage damage constitutive model is established. The model, existing model, and test curves were compared, and four indicators were introduced to evaluate the fitting effect. The results demonstrate that the stress–strain curve has a near horizontal step before the elastic stage, and its length is positively correlated with the moisture content $\omega$. With the increase in $\omega$, the peak strain increases linearly, and the compressive strength and Young's modulus first increase and then decrease. The loading rate does not change the type of the fitting function between the mechanical parameters and $\omega$. The three-stage model is more universal and can better fit the full stress–strain curve of water-bearing coal under uniaxial compression.

**Keywords:** water-bearing coal; coal sample; mechanical property; uniaxial compression; damage constitutive model



**Citation:** Ju, F.; Wang, D.; Wang, Z.; Xiao, M.; He, Z.; Ning, P.; Wang, T.; Zhou, C.; Zhang, Y.; Li, L.; et al. Research on Mechanical Properties and Damage Constitutive Model of Water-Bearing Coal. *Appl. Sci.* **2022**, *12*, 8811. https://doi.org/10.3390/app12178811

Academic Editor: Ricardo Castedo

Received: 10 August 2022
Accepted: 31 August 2022
Published: 1 September 2022



## 1. Introduction

Coal is a sedimentary rock composed of organic and inorganic materials that plays an essential role in the global energy structure as a relatively inexpensive and abundant fossil fuel [1,2]. In many developing countries, coal is the primary energy source. For example, 2.74 billion tons of coal were consumed in China in 2018, providing 59% of the country's overall primary energy usage [3]. Ensuring coal mine safety in production has positive relevance for global energy security and steady supply. In the practice of coal mining, coal seam water injection operations are carried out to prevent rock bursts, suppress gas emissions, and reduce the dust concentration at the working face; waterproof coal pillars are laid out to prevent mine water from entering the roadway; and hard top coal is hydraulically fractured for effective top coal cave mining [4–10]. Variable degrees of water–rock interaction will occur between water and coal in the above water-related engineering, resulting in the deterioration of coal's mechanical properties and concealing threats to production safety [11–13]. It is necessary to investigate the macroscopic mechanical properties and damage constitutive model of water-bearing coal for safe mining.

Scholars have conducted many studies on the macroscopic mechanical properties of water-bearing coal. Poulsen et al. [14], Perera et al. [15], and Vishal [16] investigated the attenuation law of strength and the elastic modulus of saturated coal samples through uniaxial compression experiments. Wang et al. [17] investigated the strength of saturated water-bearing coal samples versus natural water-bearing coal samples under uniaxial and triaxial compression, discovering that the former is always weaker than the latter. Yao et al. [18] performed uniaxial compression experiments on coal samples with four moisture contents and investigated the link between moisture content and mechanical properties of coal samples and crack propagation characteristics. Qin et al. [19] investigated the impact of water on the mechanical properties and acoustic emission characteristics of raw coal samples by loading experiments, and they discovered that as moisture content increased, the uniaxial compressive strength of the coal samples and the cumulative ring count of acoustic emission gradually decreased. Feng et al. [20], Yao et al. [21], Zhang et al. [22], and Liu et al. [23] also obtained similar experimental results: the uniaxial compressive strength and Young's modulus of coal samples decline monotonically as moisture content rises. Wang et al. [24], Wang et al. [25], and Zhu et al. [26] performed uniaxial compression experiments on briquette coal samples varying in moisture content and found that with increasing moisture content, the mechanical strength indexes such as uniaxial compressive strength (UCS) and Young's modulus first increased and then decreased, which were different from the experimental phenomena of raw coal samples [19–23]. There was no systematic study of the difference between the two experimental phenomena. The authors hypothesized that the difference was related to the porosity and permeability of the coal samples, and that the mechanical strength index of the water-bearing coal samples with higher porosity and permeability would first grow and subsequently decline. In this paper, raw coal samples with large porosity and high permeability are selected for uniaxial compression tests at different loading rates to explore the macroscopic mechanical properties of water-bearing coal.

At present, there is little basic research on the damage constitutive models of water-bearing coal, and some researchers have developed some damage constitutive models of water-bearing hard rock. Krajcinovic et al. [27] developed a statistical damage constitutive model suitable for rock and other materials by integrating the continuous damage concept with the statistical strength concept for the first time. Hu et al. [28], Zhou et al. [29], and Bian et al. [30] established the continuous damage constitutive models of red sandstone, shale, and sandstone considering the influence of water content. Liu et al. [31] established a logistic equation-based continuous damage model, which can fit the uniaxial compression stress–strain curves of various types of rocks. Wang et al. [32] established the two-stage discontinuous damage constitutive model of ordinary water-bearing coal recently. The two-stage model uses a piecewise function to describe the constitutive relationship of ordinary water-bearing coal, which has a better fitting effect than the traditional continuous model. Coal is a special soft rock with low strength [33], and the stress–strain curve of water-bearing coal with large porosity and high permeability used in this work is more obvious in the initial compaction stage due to the water–rock interaction, so the existing continuous model and two-stage discontinuous model are not fully applicable, and the theoretical value of the existing damage constitutive model will have a large deviation from the experimental value in the compaction stage. Therefore, this paper establishes a more accurate three-segment damage constitutive model of water-bearing coal with large porosity and high permeability to improve the fitting effect of the theoretical curve on the experimental curve.

In this article, first, uniaxial compression experiments of raw coal specimens with five water contents are performed at four loading rates. Secondly, the stress–strain properties of water-bearing coal specimens under loading are investigated, and the link between water content and mechanical parameters of coal specimens is obtained. Finally, the piecewise water-bearing coal damage constitutive model is established, and the model is validated

by experimental data. The research results are predicted to supplement the rock damage mechanics theory and improve the safety of mining in coal mines.

## 2. Experimental Methods

### *2.1. Experimental System*

#### 2.1.1. Electro-Hydraulic Servo Universal Testing Machine

As depicted in Figure 1, the press utilized in the tests in this work is a WAW-1000D microcomputer-controlled electro-hydraulic servo universal testing machine, which is manufactured by Xinte Testing Machine Co., Ltd., Changchun City, China. The machine is constituted of the host, servo controller, computer system, and servo oil source, which can automatically control force, displacement, and deformation in various modes.

**Figure 1.** The WAW-1000D microcomputer-controlled electro-hydraulic servo universal testing machine.

The technical parameters of the testing machine are as follows: the maximum experiment force is 1000 kN, the accuracy of the test force indication is less than ±1%, the experiment force measuring limit is 2% to 100% of the maximum experiment force, the isokinetic stress control limit is 2~60 $N/mm^2 \cdot S^{-1}$, the steady velocity strain control limit is 0.00025~0.0025/s, the steady velocity displacement control limit is 0.5~50 mm/min, and the maximum compression test space is 600 mm.

#### 2.1.2. Strain Measurement System

The static strain meter was applied to quantify the axial and lateral strains of the specimen during compression. As depicted in Figure 2, the strain meter model is ASMB2-8, having eight monitoring channels. It was independently developed by Sigma Company in Jinan City, Shandong Province, China, and can measure static strain with high precision.


**Figure 2.** The ASMB2-8 static strain meter.

The mass of the static strain meter is 1340 g, and its size is 191 mm × 200 mm × 79 mm. Its main technical parameters are as follows: the test range is −60,000~+60,000 με, the maximum sampling rate of the channel is 10 S/s, there are three strain resolutions (0.1/0.5/1.0 με), the test error is 0.05%D ± 0.3 με (D is the strain measurement value), and the working temperature is −40~70 °C.

### *2.2. Sample Preparation*

The coal blocks used to prepare the samples were extracted from 11,215 working faces of the main coal seam in a mine in Yulin City, China. The ZS-100 rock coring machine (Jinan Mining and Rock Testing Instrument Co., Ltd., Jinan, China) was used to drill the core along the vertical bedding direction of the coal block, and then the obtained coal core was processed into the standard raw coal sample ($\phi$50 mm × 100 mm) shown in Figure 3 through cutting, grinding, and other processes. The processing error of the coal sample meets the tolerance requirements of the standard GB/T 23561.7-2009. The mass and wave velocity of the coal samples were measured using an electronic balance and an acoustic wave instrument to ensure sample uniformity, and coal samples with minor dispersion were chosen for experiments.

**Figure 3.** The standard raw coal samples.

The preparation steps for coal samples with varying water content are as follows:

1. The coal sample selected by mass and wave velocity was put in a steady temperature drying oven, and the drying temperature was set at 105 °C. After 12 h, the heated coal sample was moved to the dryer and cooled to room temperature to measure the mass $m_{dry}$ of the dried coal sample;

2. The dried coal sample obtained by the first step was heated in a boiling vessel for eight hours and then cooled to room temperature. Finally, the coal sample was wiped off the surface water to measure its mass $m_{sr}$. The following formula can be used to calculate the saturated moisture content of a coal sample:

$$\omega_{sr} = \frac{m_{sr} - m_{dry}}{m_{dry}} \times 100\% \quad (1)$$

3. The water-saturated coal sample obtained in the second step was heated in a constant temperature and humidity drying oven, and the drying temperature was set at 40 °C. The mass of coal sample $m_w$ was measured every 30 min and the moisture content of the coal sample was calculated. When the water content of the coal sample was close to the set water content, the measurement time interval was shortened to five minutes until the coal sample reached the planned moisture content. The following is the formula for calculating the moisture content of a coal sample:

$$\omega = \frac{m_w - m_{dry}}{m_{dry}} \times 100\% \quad (2)$$

### 2.3. Experimental Scheme

The experiment consisted of four parallel test groups, each with five moisture content levels, including dry state ($\omega = 0\%$), saturated state ($\omega = 13.14\%$), natural moisture state ($\omega = 3.31\%$), and two unsaturated moisture states ($\omega = 7.06\%$ and $\omega = 10.34\%$). As shown in Table 1, the water contents of the four parallel test groups were approximately equal, and their ranges were 0~13.37% (S1), 0~13.55% (S2), 0~13.31% (S3), and 0~13.85% (S4), respectively. According to the research results of Qi et al. [34], the water content of coal seams is mostly lower than 15%, so the water content set in this paper is consistent with the actual situation.

**Table 1.** The water content of coal samples was tested in four parallel test groups.

| Test Group | Number | $m_w$/g | $m_{dry}$/g | $\omega$/% |
|---|---|---|---|---|
| S1 | S1-1 | 244.8 | 238.4 | 0 |
| | S1-2 | 245.2 | - | 3.31 |
| | S1-3 | 238.4 | 231.2 | 7.09 |
| | S1-4 | 255.2 | 248.3 | 10.31 |
| | S1-5 | 244.1 | 237.1 | 13.37 |
| S2 | S2-1 | 256.3 | 249.1 | 0 |
| | S2-2 | 243.5 | - | 3.31 |
| | S2-3 | 245.1 | 238.5 | 7.09 |
| | S2-4 | 247.0 | 239.9 | 10.75 |
| | S2-5 | 250.5 | 243.6 | 13.55 |
| S3 | S3-1 | 241.4 | 234.0 | 0 |
| | S3-2 | 245.1 | - | 3.31 |
| | S3-3 | 236.3 | 229.9 | 7.05 |
| | S3-4 | 254.0 | 246.6 | 10.42 |
| | S3-5 | 250.7 | 243.4 | 13.31 |
| S4 | S4-1 | 263.5 | 256.7 | 0 |
| | S4-2 | 245.8 | - | 3.31 |
| | S4-3 | 247.2 | 240.6 | 7.07 |
| | S4-4 | 240.6 | 233.5 | 10.49 |
| | S4-5 | 252.8 | 245.4 | 13.85 |

The test system's schematic diagram is depicted in Figure 4, and the test loading method used in this article is displacement loading. A resistance strain gauge was used to measure the axial and transverse strains of coal samples at the same time. The four

parallel test groups (S1, S2, S3, and S4) were subjected to four loading rates (0.05 mm/min, 0.10 mm/min, 0.20 mm/min, and 0.50 mm/min) until the coal samples were destroyed.

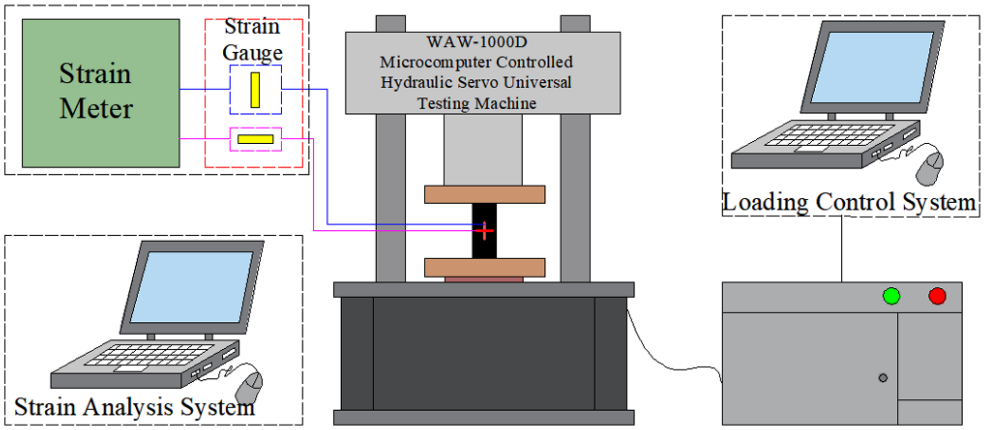


**Figure 4.** The schematic diagram of the test system.

## 3. Experimental Results

### *3.1. Uniaxial Compressive Stress–Strain Characteristics of Coal Samples*

The uniaxial compression stress–strain curves of coal samples with varying water contents are shown in Figure 5. When the results of four parallel test groups are compared, the pre-peak stress–strain curves of coal samples are found to be very similar, but the peak stress–strain curves are significantly different, indicating a degree of discreteness.

The mechanical properties and deformation characteristics of the four parallel test groups' four groups of coal samples with various water contents show consistent fluctuation trends. The maximum values of the uniaxial compressive strength and Young's modulus of coal samples are reached when the coal sample has a natural moisture content, while the maximum strain of coal samples rises monotonically with increasing moisture content. As an illustration, in test group S1, coal sample moisture content increased from 0% to 3.31%, compressive strength increased from 6.42 MPa to 12.61 MPa, and peak strain increased from 1.60% to 1.63%; in test group S2, coal sample moisture content increased from 3.31% to 13.14%, compressive strength decreased from 12.61 MPa to 6.23 MPa, and peak strain increased from 1.63% to 2.14%.

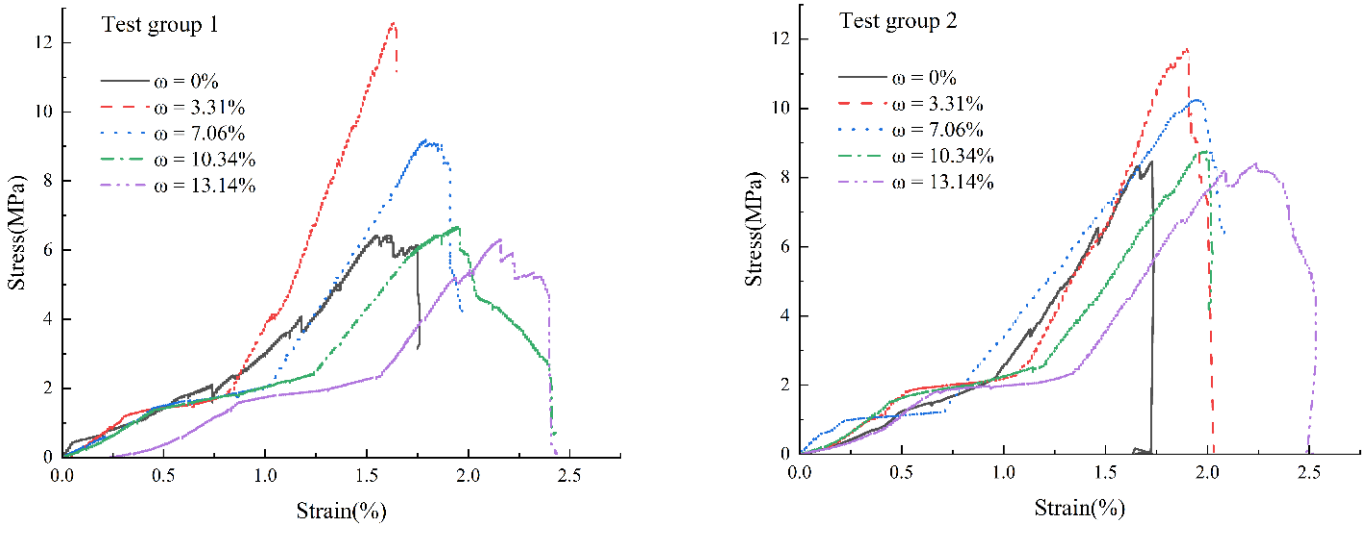


(**a**) (**b**)

**Figure 5.** *Cont.*

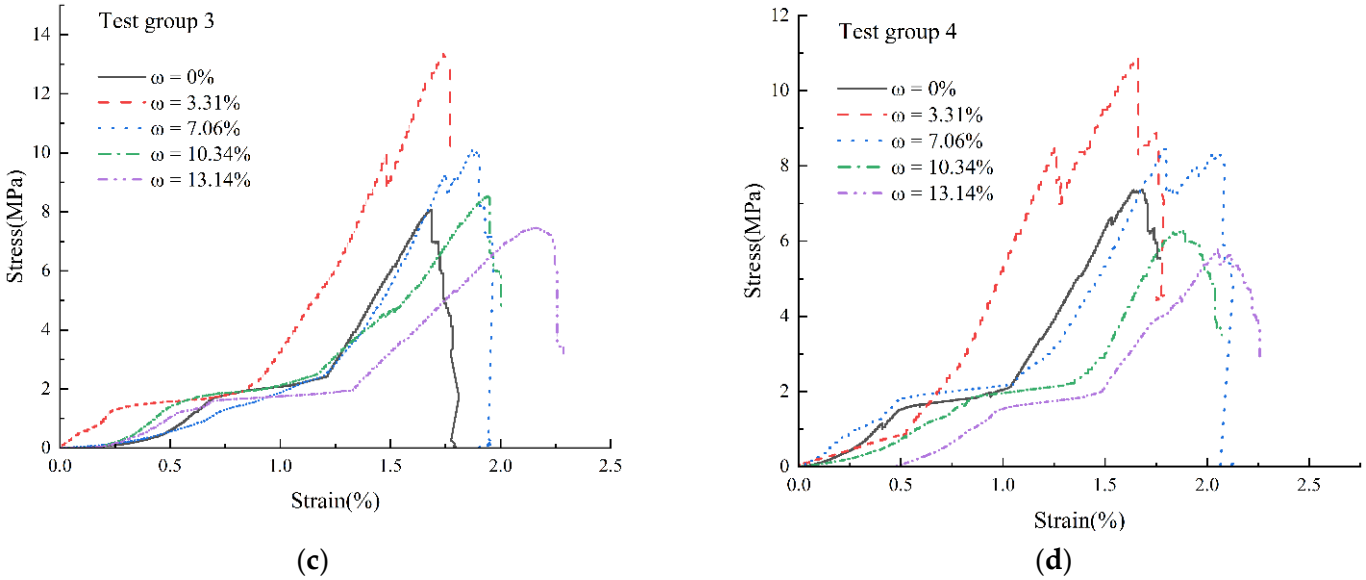


**Figure 5.** Uniaxial compressive stress–strain curves of coal samples of different moisture content. (**a**) Loading rate: 0.05 mm/min; (**b**) loading rate: 0.10 mm/min; (**c**) loading rate: 0.20 mm/min; (**d**) loading rate: 0.50 mm/min.

The stress–strain curves of coal samples with varying moisture content all have a near horizontal step between the fracture compaction stage and the elastic deformation stage, which is referred to in this paper as the pore compaction stage. As a result, the stress–strain curve has five stages: fracture compaction, pore compaction, elastic deformation, plastic deformation, and post-peak failure. From Figure 5a–d, it can be found that the stress–strain curve of the dry coal sample exhibits linear elastic change before the peak, axial stress drops rapidly in linear form after the peak point, and there is almost no falling platform. The fracture and pore compaction stage intervals increase significantly as the moisture content of coal samples increases, the elastic stage interval decreases, and the plastic deformation stage becomes more obvious. In addition, as the water content increases, the axial stress drop velocity after the peak point decreases, revealing a multi-level drop platform.

From Figure 5a–d, it can be found that with an increase in water content, the near horizontal step becomes longer, and the interval of the pore compaction stage increases. We believe that this phenomenon may be related to the particularity of the test coal samples. Scholars discovered that coal has a porous structure through CT scans and three-dimensional reconstruction [35], and some researchers discovered that the porosity and permeability of the coal seam sampled in this test are large [36,37], resulting in the internal micro-pores of coal samples being filled with water after immersion, as shown in Figure 6. The coal sample's micro-cracks closed at the start of loading, the coal sample gradually became more compact as the axial strain increased, its elastic modulus rose as well, and the stress–strain curve was concave upward in this stage. The hydrostatic pressure in the coal sample's micro-pores increased as the external load increases, resulting in micro-pore rupture and a large number of micro-damages in the coal sample. The stress changes are minor at this stage, but the strain develops quickly, and the stress–strain curve appears near the horizontal step. Because the number of micro-damages is positively correlated with water content, the degree of internal damage in coal samples with higher water content is greater than in coal samples with lower water content, and the interval length of the pore compaction stage in coal samples with higher moisture content is also larger than in coal samples with lower water content.

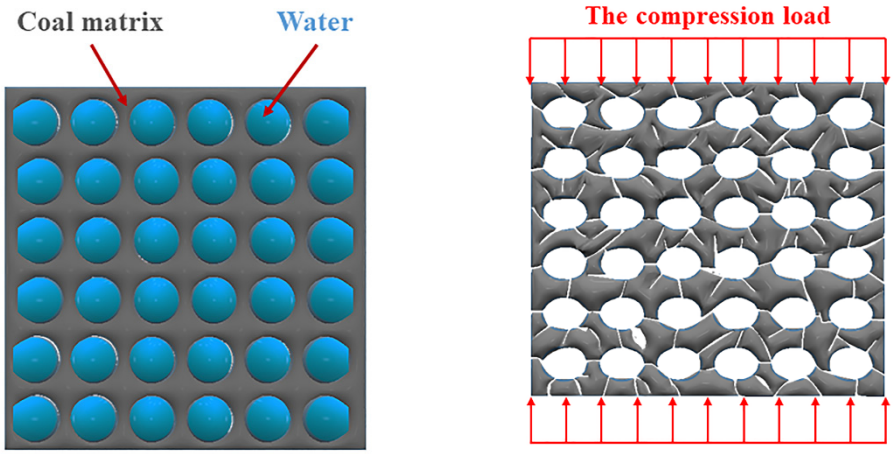


**Figure 6.** A diagram of the water filling and compression failure of the coal micro-pore structure. (**a**) Water filling of pore structure; (**b**) compression failure of pore structure.

### *3.2. Relationship between Mechanical Parameters and Moisture Content of Coal Samples*

By analyzing the measured data of the uniaxial compression test of the coal samples, the specific values of mechanical parameters (compressive strength, Young's modulus, and peak strain) of coal samples with different water content can be obtained.

Figure 7 shows the fitting curves for the mechanical parameters and moisture content of the coal samples in four parallel test groups. It was discovered that the coal samples in each test group can be fitted by the same functional relationship with a high degree of accuracy. Therefore, it can be considered that the loading rate does not change the type of fitting function for each of the mechanical parameters.

The function expressions of uniaxial compressive strength $\sigma_c$, Young's modulus $E$, peak strain $\varepsilon_c$, and moisture content $\omega$ of coal samples are as follows:

$$\begin{cases} \sigma_c = a_1 + b_1\omega + b_2\omega^2 + b_3\omega^3 \\ E = a_2 + b_4\omega + b_5\omega^2 + b_6\omega^3 \\ \varepsilon_c = \varepsilon_0 + k\omega \end{cases} \quad (3)$$

In Equation (3), $a_1 \sim a_6$, $b_1$, $b_2$ and $k$ are fitting parameters, and $\varepsilon_0$ is the peak strain of a dry coal sample.

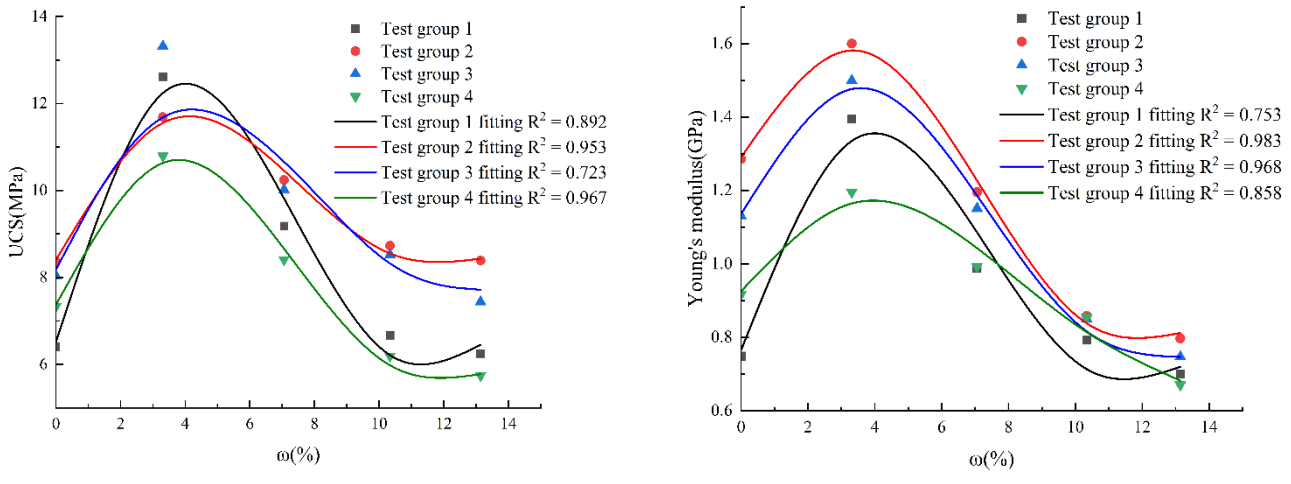


**Figure 7.** *Cont.*

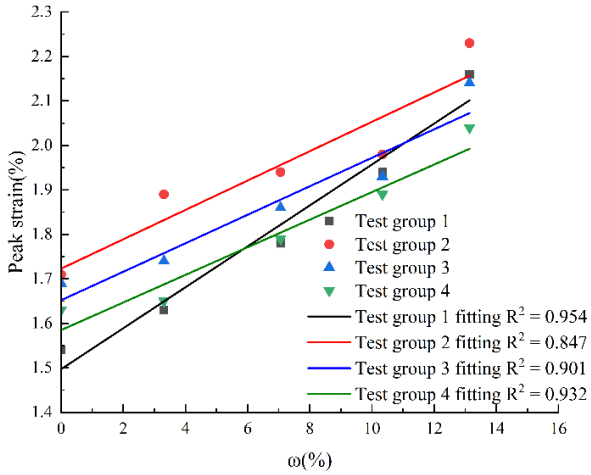


(**c**)

**Figure 7.** The fitting curve of mechanical parameters and moisture content of coal samples: (**a**) uniaxial compressive strength; (**b**) Young's modulus; (**c**) peak strain.

## 4. Damage Constitutive Model

### *4.1. Evolution Law of Mesoscopic Damage*

#### 4.1.1. Mesoscopic Damage Caused by Water–Rock Interaction

The water–rock interaction process is represented in Figure 8. Generally, the mesoscopic damage to coal in the water–rock interaction can be roughly divided into two categories: physical damage and chemical damage [13]. Physical damage causes colloids that hold mineral particles together to dissolve, weakening the cohesiveness between the particles and causing the particles to wash out of the coal body. Chemical damage causes soluble materials to dissolve in acidic and alkaline aqueous solutions. The coal mass's macroscopic mechanical characteristics alter as a result of the coal mass's microstructure changing due to the water–rock interaction.

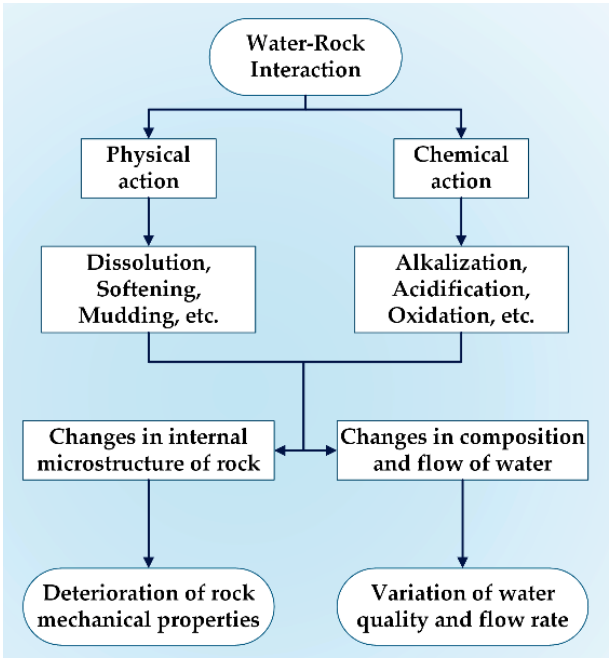


**Figure 8.** The schematic diagram of the water–rock interaction process.

Considering that the Young's modulus of rock materials is easy to measure and analyze during the water–rock interaction process, the damage variable $D_1$ of coal samples caused by the water–rock interaction can be expressed as:

$$D_1 = 1 - \frac{E_\omega}{E_0} \tag{4}$$

In Equation (4): $E_0$ is the Young's modulus of coal with initial natural moisture content, and $E_\omega$ is the Young's modulus of coal sample with moisture content $\omega$.

As the moisture content of coal increases, the damage degree caused by the water–rock interaction is intensified, Young's modulus is gradually reduced, and the damage variable $D_1$ is gradually increased. Therefore, the evolution law of the damage caused by the water–rock interaction can be obtained with water content as a control variable.

4.1.2. Mesoscopic Damage Caused by Loading

The distribution of the mineral particles' physical and mechanical characteristics in coal is random, so the strength of the micro-element body in coal can be considered to meet a specific statistical distribution type, and hence it is possible to establish the coal's statistical damage constitutive model.

Scholars have introduced a variety of micro-element strength distribution types in their studies, including dual-parameter Weibull distribution, logarithmic normal distribution, normal distribution, and power function distribution. Studies have shown that the fitting effect of the two-parameter Weibull distribution is better than that of other distribution types [38]. Therefore, this paper assumes that the strength of the micro-element body in coal follows this distribution, and its probability density function is [39]:

$$P(S) = \frac{m}{n}\left(\frac{S}{n}\right)\exp\left[-\left(\frac{S}{n}\right)^m\right] \tag{5}$$

In Equation (5): $P(S)$ is the strength distribution function of a coal sample micro-element; $S$ is the random distribution variable of micro-element strength, it is a combined function of stress, known as stress level; and $m$ and $n$ are distribution parameters obtained by analyzing the experimental data.

When the stress of the coal rises to a particular degree, the number of damaged micro-elements inside the coal is:

$$N' = \int_0^S NP(x)\mathrm{d}x = N\left\{1 - \exp\left[-\left(\frac{S}{n}\right)^m\right]\right\} \tag{6}$$

In Equation (6): $N$ is the total number of micro-elements in coal and rock and $N'$ is the number of damaged micro-elements.

The number of damaged micro-elements divided by the total number of micro-elements is the damage variable $D_2$ of the coal under load:

$$D_2 = \frac{N'}{N} \tag{7}$$

The equation for the damage evolution of the coal under loading is obtained by substituting Equation (6) into Equation (7):

$$D_2 = 1 - \exp\left[-\left(\frac{S}{n}\right)^m\right] \tag{8}$$

4.1.3. Evolution of Total Mesoscopic Damage

The first damaged state of coal is defined as the state in which only the water–rock interaction takes place, while the second damaged state is described as the state in which

coal is only loaded. The one-dimensional constitutive relations of coal under two damage states are as follows:

$$\sigma_\omega = E_0(1 - D_1)\varepsilon_\omega \tag{9}$$

$$\sigma = E_\omega(1 - D_2)\varepsilon \tag{10}$$

In Equations (9) and (10), $\sigma_\omega$ and $\varepsilon_\omega$ are stress and strain caused by the water–rock interaction respectively; $\sigma$ and $\varepsilon$ are stress and strain caused by the load, respectively.

According to Lemaitre's equivalent strain hypothesis [40] and Zhang et al.'s generalized strain equivalence principle [41], the one-dimensional constitutive model of water-bearing coal under loading can be obtained by solving Equations (4), (9) and (10):

$$\sigma = E_0(1 - D)\varepsilon \tag{11}$$

In Equation (11): $D$ is the total damage of a coal sample caused by the water–rock interaction combined with load, and its expression is:

$$D = D_1 + D_2 - D_1D_2 \tag{12}$$

It can be seen from Equation (12) that the dual impact of the water–rock interaction and load increase the overall mesoscopic damage of coal, but the total mesoscopic damage is not a simple superposition of two basic damages, and the coefficient of the coupling term $D_1D_2$ is negative, indicating that the coupling effect reduces the total mesoscopic damage. We conclude that this may be because the mesoscopic damage caused by the water–rock interaction increases the mesoscopic defects in the coal mass, and, to a certain extent, increases the threshold of dislocation movement under load in the coal body. After loading, the micro-pores and micro-cracks in coal are sealed, and the mesoscopic damage caused by the water–rock interaction is reduced.

From Equations (4), (8) and (12), the total mesoscopic damage evolution equation of water-bearing coal under loading can be obtained:

$$D = 1 - \frac{E_w}{E_0}\left\{1 - \exp\left[-\left(\frac{S}{n}\right)^m\right]\right\} \tag{13}$$

According to Equation (13), when only the damage resulting from the water–rock interaction is considered, there is $S = 0$, and $D = D_1$; when only the damage caused by loading is considered, there is $E_w = E_0$, and $D = D_2$.

### *4.2. Random Distribution Variable of Micro-Element Strength*

To derive the damage constitutive equation of coal, it is important to identify the precise expression of $S$ in Equation (13). In this paper, the Drucker–Prager strength criterion commonly used in geotechnical materials is used as a reference.

The expression of the random distribution variable $S$ of the micro-element strength corresponding to the Drucker–Prager strength criterion is:

$$S = \alpha I_1^* - \sqrt{J_2^*} \tag{14}$$

In Equation (14): $I_1^*$ is the first principal invariant of the effective stress tensor, $J_2^*$ is the second principal invariant of the effective stress deviation, and $\alpha$ is the material parameter. The following equations can be used to calculate $I_1^*$ and $J_2^*$:

$$I_1^* = \sigma_1^* + \sigma_2^* + \sigma_3^* \tag{15}$$

$$J_2^* = \frac{(\sigma_1^* - \sigma_2^*)^2 + (\sigma_2^* - \sigma_3^*)^2 + (\sigma_3^* - \sigma_1^*)^2}{6} \tag{16}$$

According to the equivalent strain hypothesis [40], the relationship between effective stress and nominal stress is as follows:

$$\sigma_i^* = \frac{\sigma_i}{1-D}(i = 1,2,3) \tag{17}$$

From Equations (14)–(17), the expression of random distribution variable $S$ can be obtained:

$$S = \frac{(\alpha I_1 + \sqrt{J_2})E\varepsilon_1}{\sigma_1 - \mu(\sigma_2 + \sigma_3)} \tag{18}$$

In Equation (18): $I_1$ is the first principal invariant of the nominal stress tensor, $J_2$ is the second principal invariant of the nominal stress deviation. $I_1$ and $J_2$ can be calculated by the following equations:

$$I_1 = \sigma_1 + \sigma_2 + \sigma_3 \tag{19}$$

$$J_2 = \frac{(\sigma_1 - \sigma_2)^2 + (\sigma_2 - \sigma_3)^2 + (\sigma_3 - \sigma_1)^2}{6} \tag{20}$$

In the case of uniaxial compression, there are $\sigma_1 = \sigma$, $\sigma_2 = \sigma_3 = 0$, $\varepsilon_1 = \varepsilon$, and Equation (18) can be simplified:

$$S = \left(\alpha + \frac{1}{\sqrt{3}}\right)E\varepsilon \tag{21}$$

### *4.3. Sectional Damage Constitutive Model*

Referring to the research results of Lu [42], the one-dimensional constitutive relation of water-bearing coal in the fracture compaction stage can be defined as:

$$\sigma = \sigma_a\left(\frac{\varepsilon}{\varepsilon_a}\right)^2 \tag{22}$$

In Equation (22): $\sigma_a$ and $\varepsilon_a$ are the maximal stress and strain in the fracture compaction stage of water-bearing coal under uniaxial compression.

Figure 3 shows that the stress–strain curve of water-bearing coal during the pore compaction stage is nearly horizontal, so the one-dimensional constitutive model in this stage can be defined as:

$$\sigma = \sigma_a + \frac{\sigma_b - \sigma_a}{\varepsilon_b - \varepsilon_a}(\varepsilon - \varepsilon_a) \tag{23}$$

In Equation (23): $\sigma_b$ and $\varepsilon_b$ are the maximal stress and strain in the pore compaction stage of water-bearing coal under uniaxial compression.

From Equations (13), (15) and (21), the one-dimensional constitutive model of water-bearing coal in elastic deformation, plastic deformation, and post-peak failure stages can be obtained:

$$\sigma = \sigma_b + E_\omega(\varepsilon - \varepsilon_b)\exp\left\{-\left[\frac{\left(\alpha + \frac{1}{\sqrt{3}}\right)E_\omega\varepsilon}{n}\right]^m\right\} \tag{24}$$

At the peak point ($\varepsilon_c$, $\sigma_c$), the uniaxial compression stress–strain curve meets the boundary requirements: (1) $\varepsilon = \varepsilon_c$, $\sigma = \sigma_c$; (2) $\varepsilon = \varepsilon_c$, $\frac{\partial\sigma}{\partial\varepsilon} = 0$. Substituting the boundary conditions into Equation (24), the expression of $m$ and $n$ can be obtained after solving:

$$m = \frac{\varepsilon_c}{R(\varepsilon_b - \varepsilon_c)} \tag{25}$$

$$n = \left(\alpha + \frac{1}{\sqrt{3}}\right)E_\omega\varepsilon_c(-R)^{-\frac{1}{m}} \tag{26}$$

For the specific stress–strain curve, $R$ is a constant in Equations (25) and (26), and its calculation equation is as follows:

$$R = \ln \frac{\sigma_c - \sigma_b}{E_\omega(\varepsilon_c - \varepsilon_b)} \tag{27}$$

The expressions of $m$ and $n$, namely Equations (25) and (26), are substituted into Equation (24), and the subsequent equation can be derived:

$$\sigma = \sigma_b + E_\omega(\varepsilon - \varepsilon_b) \exp\left[R\left(\frac{\varepsilon}{\varepsilon_c}\right)^{\frac{\varepsilon_c}{R(\varepsilon_b - \varepsilon_c)}}\right] \tag{28}$$

By combining Equations (21), (22) and (26), the segmented damage constitutive model of water-bearing coal can be obtained:

$$\sigma = \begin{cases} \sigma_a\left(\dfrac{\varepsilon}{\varepsilon_a}\right)^2 & (\varepsilon < \varepsilon_a) \\ \sigma_a + \dfrac{\sigma_b - \sigma_a}{\varepsilon_b - \varepsilon_a}(\varepsilon - \varepsilon_a) & (\varepsilon_a \le \varepsilon < \varepsilon_b) \\ \sigma_b + E_\omega(\varepsilon - \varepsilon_b) \exp\left[R\left(\dfrac{\varepsilon}{\varepsilon_c}\right)^{\frac{\varepsilon_c}{R(\varepsilon_b - \varepsilon_c)}}\right] & (\varepsilon \ge \varepsilon_b) \end{cases} \tag{29}$$

## 5. Validation of the Constitutive Model

The constitutive model developed in Section 4 is validated using the experimental data collected in Section 3. Wang et al. [32] assumed that the strength of the coal micro-element body obeyed the distribution of the power function, and on this basis, the two-stage damage constitutive model of water-bearing coal was deduced. The model of Wang et al. [32] was used to calculate the test results in this article, and the two models' fitting results were compared and analyzed.

The fitting results of the two models are shown in Figures 9–12.

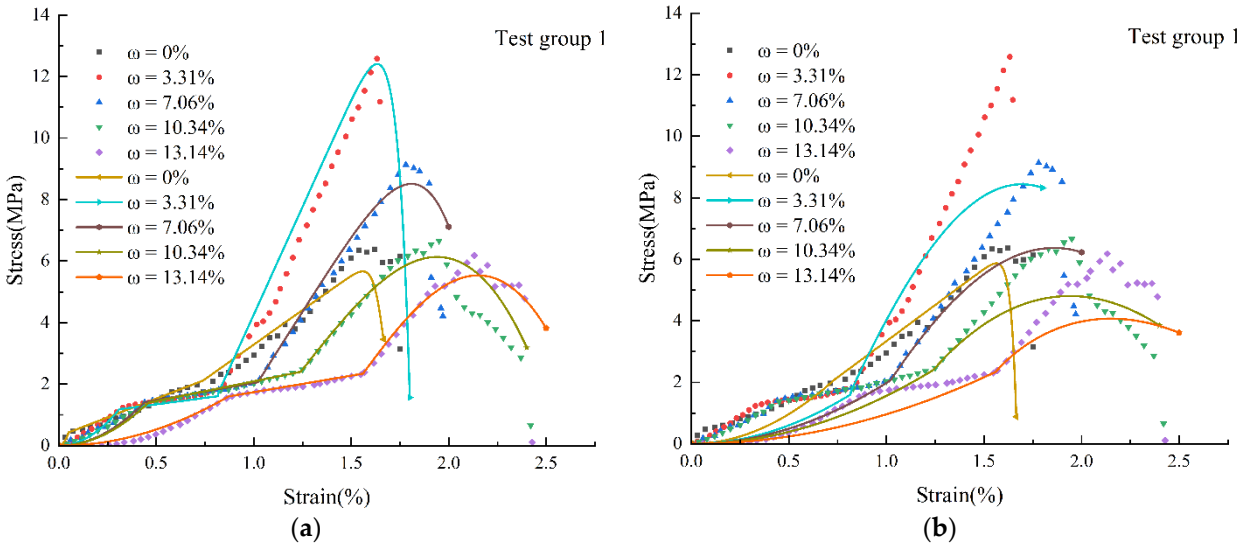


**Figure 9.** The uniaxial compression test data points and theoretical model curve of coal samples in test group 1: (**a**) the author's model; (**b**) the comparison model.

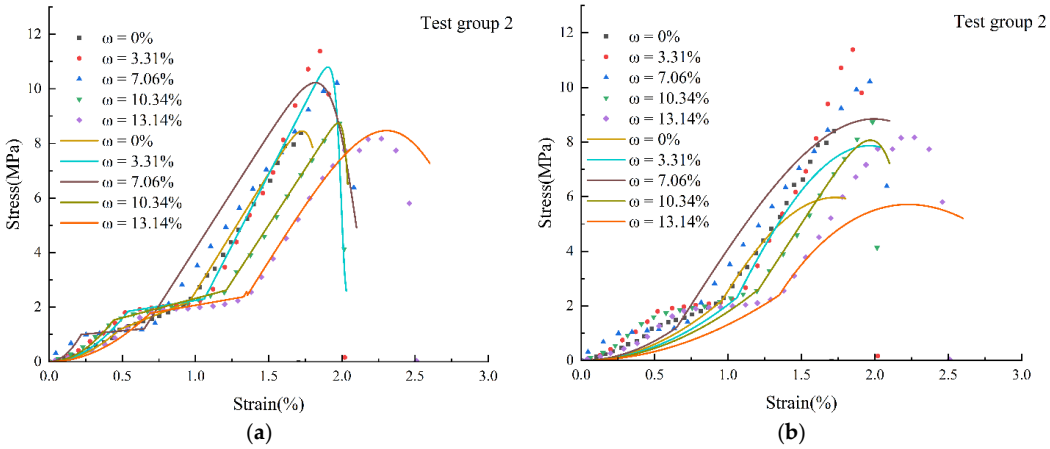


**Figure 10.** The uniaxial compression test data points and theoretical model curve of coal samples in test group 2: (**a**) the author's model; (**b**) the comparison model.

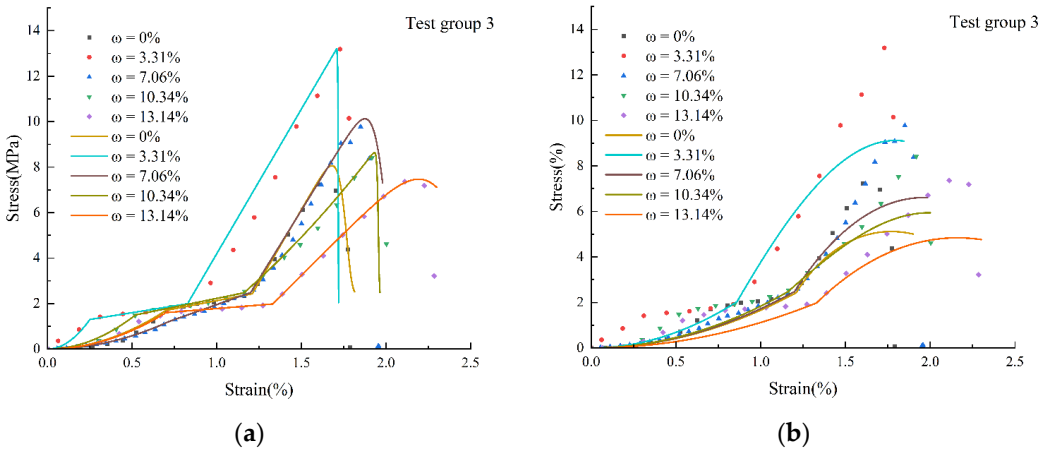


**Figure 11.** The uniaxial compression test data points and theoretical model curve of coal samples in test group 3: (**a**) the author's model; (**b**) the comparison model.

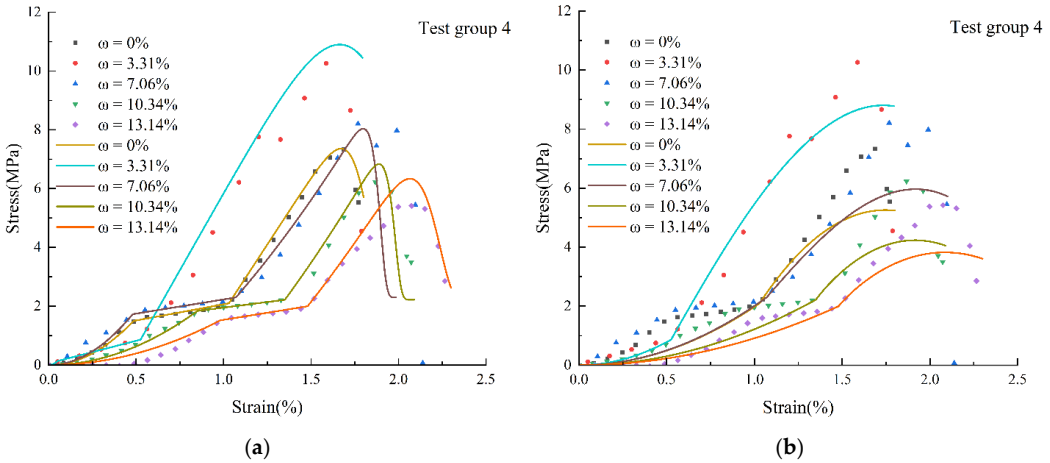


**Figure 12.** The uniaxial compression test data points and theoretical model curve of coal samples in test group 4: (**a**) the author's model; (**b**) the comparison model.

In the study literature on the coal (rock) constitutive model, there are few indications to quantitatively assess the fitting result of the constitutive model. To scientifically evaluate the fitting effect of the damage constitutive model, the following four statistical indicators are introduced in this paper:

1. Mean absolute error (MAE), which is defined as:

$$\mathrm{MAE}(y,\hat{y}) = \frac{1}{l}\sum_{i=1}^{l}(|y_i - f(x_i)|) \tag{30}$$

2. Mean square error (MSE), which is defined as:

$$\mathrm{MSE}(y,\hat{y}) = \frac{1}{l}\sum_{i=1}^{l}(y_i - f(x_i))^2 \tag{31}$$

3. Root mean square error (RMSE), which is defined as:

$$\mathrm{RMSE}(y,\hat{y}) = \sqrt{\frac{1}{l}\sum_{i=1}^{l}(y_i - f(x_i))^2} \tag{32}$$

4. Decision coefficient ($R^2$), which is defined as:

$$R^2 = 1 - \frac{\mathrm{MSE}(y,\hat{y})}{\frac{1}{l}\sum_{i=1}^{l}(y_i - \overline{y})^2} \tag{33}$$

In Equations (30)–(33): $y$ is the parameter to be estimated, it is the strength of the coal sample in this paper, and $\hat{y}$ is the estimator of $y$; $l$ is the number of statistical samples; $y_i$ is the true value of the test data; $f(x_i)$ is the predicted value of the damage constitutive model; $\overline{y}$ is the average amount of the test data.

The MAE, MSE, and RMSE can reflect the deviation between the experimental amount and the theoretical amount of the model; the smaller the value is, the higher the fitting degree of the model is, and when the value is zero, the experimental value is equal to the theoretical value, and the damage constitutive model is the perfect model. The value of $R^2$ can reflect the degree of approximation of the theoretical value of the model to the real test value; the larger the value is, the better the model fitting effect is. The fitting effect evaluation indexes (MAE, MSE, RMSE, and $R^2$) corresponding to the three-stage damage constitutive model in this paper and Wang et al.'s [32] two-stage damage constitutive model are shown in Tables 2–5.

**Table 2.** The fitting effect evaluation index values of the two models based on the experimental data in test group 1.

| Index | $\omega$ = 0% | | $\omega$ = 3.31% | | $\omega$ = 7.06% | | $\omega$ = 10.34% | | $\omega$ = 13.14% | |
|---|---|---|---|---|---|---|---|---|---|---|
| | The Authors' Model | The Comparison Model | The Authors' Model | The Comparison Model | The Authors' Model | The Comparison Model | The Authors' Model | The Comparison Model | The Authors' Model | The Comparison Model |
| MAE | 0.507 | 0.476 | 0.683 | 0.894 | 0.057 | 0.682 | 0.595 | 0.665 | 1.059 | 0.580 |
| MSE | 0.429 | 0.618 | 0.869 | 1.681 | 0.008 | 0.825 | 0.775 | 0.666 | 1.916 | 0.668 |
| RMSE | 0.655 | 0.786 | 0.932 | 1.296 | 0.092 | 0.908 | 0.881 | 0.816 | 1.384 | 0.817 |
| $R^2$ | 0.89 | 0.84 | 0.94 | 0.88 | 0.99 | 0.87 | 0.81 | 0.83 | 0.51 | 0.83 |

**Table 3.** The fitting effect evaluation index values of the two models based on the experimental data in test group 2.

| Index | $\omega$ = 0% | | $\omega$ = 3.31% | | $\omega$ = 7.06% | | $\omega$ = 10.34% | | $\omega$ = 13.14% | |
|---|---|---|---|---|---|---|---|---|---|---|
| | The Authors' Model | The Comparison Model | The Authors' model | The Comparison Model | The Authors' Model | The Comparison Model | The Authors' Model | The Comparison Model | The Authors' Model | The Comparison Model |
| MAE | 0.123 | 0.459 | 0.379 | 1.148 | 0.603 | 0.638 | 0.062 | 0.421 | 0.225 | 0.839 |
| MSE | 0.028 | 0.515 | 0.572 | 4.194 | 0.615 | 0.672 | 0.006 | 0.338 | 0.280 | 1.341 |
| RMSE | 0.168 | 0.718 | 0.756 | 2.048 | 0.784 | 0.820 | 0.077 | 0.581 | 0.529 | 1.158 |
| $R^2$ | 0.99 | 0.92 | 0.95 | 0.65 | 0.94 | 0.94 | 0.99 | 0.95 | 0.96 | 0.83 |

**Table 4.** The fitting effect evaluation index values of the two models based on the experimental data in test group 3.

| Index | $\omega$ = 0% | | $\omega$ = 3.31% | | $\omega$ = 7.06% | | $\omega$ = 10.34% | | $\omega$ = 13.14% | |
|---|---|---|---|---|---|---|---|---|---|---|
| | The Authors' Model | The Comparison Model | The Authors' Model | The Comparison Model | The Authors' Model | The Comparison Model | The Authors' Model | The Comparison Model | The Authors' Model | The Comparison Model |
| MAE | 0.282 | 0.761 | 0.834 | 0.949 | 0.231 | 0.556 | 0.688 | 0.496 | 0.345 | 0.792 |
| MSE | 0.563 | 1.840 | 4.838 | 1.949 | 0.187 | 1.067 | 1.450 | 0.538 | 1.229 | 1.203 |
| RMSE | 0.751 | 1.357 | 2.200 | 1.396 | 0.432 | 1.033 | 1.204 | 0.733 | 1.108 | 1.097 |
| $R^2$ | 0.89 | 0.64 | 0.73 | 0.89 | 0.98 | 0.89 | 0.73 | 0.90 | 0.76 | 0.77 |

**Table 5.** The fitting effect evaluation index values of the two models based on the experimental data in test group 4.

| Index | $\omega$ = 0% | | $\omega$ = 3.31% | | $\omega$ = 7.06% | | $\omega$ = 10.34% | | $\omega$ = 13.14% | |
|---|---|---|---|---|---|---|---|---|---|---|
| | The Authors' Model | The Comparison Model | The Authors' Model | The Comparison Model | The Authors' Model | The Comparison Model | The Authors' Model | The Comparison Model | The Authors' Model | The Comparison Model |
| MAE | 0.120 | 0.620 | 0.876 | 0.639 | 0.727 | 0.756 | 0.296 | 0.588 | 0.311 | 0.374 |
| MSE | 0.058 | 0.739 | 2.827 | 1.443 | 2.650 | 0.881 | 0.365 | 0.590 | 0.225 | 0.299 |
| RMSE | 0.240 | 0.860 | 1.681 | 1.201 | 1.628 | 0.939 | 0.604 | 0.768 | 0.475 | 0.547 |
| $R^2$ | 0.99 | 0.86 | 0.77 | 0.88 | 0.61 | 0.87 | 0.90 | 0.84 | 0.93 | 0.90 |

From the fitting results in Figures 9–12, it can be noticed that the three-stage constitutive model curve derived in this paper is basically identical to the experimental curve at each loading rate. By observing the values of each evaluation index in Tables 2–5, it can be found that the maximum MAE, MSE, and RMSE corresponding to the model in this paper are 1.059, 4.838, and 2.200, respectively, and the maximum $R^2$ is 0.99, indicating that the model has a high fitting degree and good applicability.

Wang et al.'s [32] model can accurately describe the changing trend of the uniaxial compression total stress–strain curve of water-bearing coal, but there are many inconsistent points. The MAE, MSE, and RMSE values of this model are generally larger than those of this model, and the $R^2$ values are mostly smaller than those of this model.

The fitting effect of the traditional continuous damage constitutive model in the fracture compaction stage of the specimen is worse than that in other stages, and there is a certain deviation between the theoretical and experimental value. Wang et al. [32] put forward a two-stage damage constitutive model by improving the continuous damage constitutive model, which has a good matching effect to the full stress–strain curve of common small porosity and low permeability coal. The three-stage damage constitutive model suggested in this study is more universal and can fit the full stress–strain curve of large porosity and high permeability coal wells. Wang et al.'s [32] model is a special form of this model; when $\sigma_b = \sigma_a$ and $\varepsilon_b = \varepsilon_a$, the model in this paper degenerates into Wang et al.'s [32] model.

## 6. Conclusions

The main conclusions are summarized as follows:

- The full stress–strain curve of coal under uniaxial compression has a nearly horizontal step before the elastic stage, which is described as the pore compaction stage in this article. The interval length of this stage is positively correlated with the water content, and this stage will only emerge with the stress–strain curve of water-bearing coal with high porosity and permeability.
- With increasing water content, the interval between the fracture compaction stage and the coal sample pore compaction stage increases, the elastic deformation stage interval decreases, the plastic failure stage is more obvious, and the multistage stress drop platform appears in the post-peak failure stage.
- The loading rate does not change the type of the fitting function between the mechanical parameters (uniaxial compression strength, Young's modulus, and peak strain)

of coal samples and their moisture content. The mechanical parameters of the coal samples in each parallel test group can be fitted as the same function as their moisture content, and all have good fitting results.

- The three-stage damage constitutive model of water-bearing coal is derived, and the statistical indicators (MAE, MSE, RMSE, and $R^2$) are introduced to scientifically evaluate the fitting effect of the model. This model improves the shortcomings of the traditional continuous fitting curve and the two-stage fitting curve. The fitting degree of the experimental curve and the theoretical curve is high, and it can better characterize and predict the mechanical properties of coal under different water contents.

**Author Contributions:** Conceptualization, F.J. and D.W.; Project administration, F.J.; Methodology, F.J., D.W. and Z.W.; Resources, F.J.; Funding acquisition, F.J.; Supervision, F.J.; Formal analysis, D.W.; Writing—Original Draft, D.W.; Writing—review and editing, D.W.; Visualization, D.W., M.X., Z.H., P.N., T.W., C.Z., Y.Z., L.L. and C.Y.; Investigation, D.W., Z.W., M.X., Z.H., P.N., T.W., C.Z., Y.Z., L.L. and C.Y. All authors have read and agreed to the published version of the manuscript.

**Funding:** This research received no external funding.

**Institutional Review Board Statement:** Not applicable.

**Informed Consent Statement:** Not applicable.

**Data Availability Statement:** Not applicable.

**Conflicts of Interest:** The authors declare no conflict of interest.

## References

1. Wolde-Rufael, Y. Coal consumption and economic growth revisited. *Appl. Energy* **2010**, *87*, 160–167. [CrossRef]
2. Balat, M. Status of fossil energy resources: A global perspective. *Energy Sources* **2007**, *2 Pt B*, 31–47. [CrossRef]
3. Xie, H.; Wu, L.; Zheng, D. Prediction on the energy consumption and coal demand of China in 2025. *J. China Coal Soc.* **2019**, *44*, 1949–1960. [CrossRef]
4. Zhou, Z.; Tan, L.; Cai, X. Water Infusion on the Stability of Coal Specimen under Different Static Stress Conditions. *Appl. Sci.* **2020**, *10*, 2043. [CrossRef]
5. Yao, Q.; Yu, L.; Chen, N.; Wang, W.; Xu, Q. Experimental Study on Damage and Failure of Coal-Pillar Dams in Coal Mine Underground Reservoir under Dynamic Load. *Geofluids* **2021**, *2021*, 5623650. [CrossRef]
6. Yang, W.; Lu, C.; Si, G.; Lin, B.; Jiao, X. Coal and gas outburst control using uniform hydraulic fracturing by destress blasting and water-driven gas release. *J. Nat. Gas Sci. Eng.* **2020**, *79*, 103360. [CrossRef]
7. Van Nguyen, D.; Nguyen, H.P.; Do, T.M. Experimental Study on the Efficacy of Water Infusion for Underground Mining of a Coal Seam. *Appl. Sci.* **2019**, *9*, 3820. [CrossRef]
8. Liu, X.; Xu, G.; Zhang, C.; Kong, B.; Qian, J.; Zhu, D.; Wei, M. Time Effect of Water Injection on the Mechanical Properties of Coal and Its Application in Rockburst Prevention in Mining. *Energies* **2017**, *10*, 1783. [CrossRef]
9. Huang, B.; Wang, Y.; Cao, S. Cavability control by hydraulic fracturing for top coal caving in hard thick coal seams. *Int. J. Rock Mech. Min. Sci.* **2015**, *74*, 45–57. [CrossRef]
10. Hu, G.; Xu, J.; Ren, T.; Dong, Y.; Qin, W.; Shan, Z. Field investigation of using water injection through inseam gas drainage boreholes to control coal dust from the longwall face during the influence of abutment pressure. *Int. J. Min. Reclam. Environ.* **2016**, *30*, 48–63. [CrossRef]
11. Zhong, Y.; Li, Q.; Wang, R.; Yao, T. Changes of Physical and Mechanical Properties of Coral Reef Limestone under $CO_2$–Seawater–Rock Interaction. *Appl. Sci.* **2022**, *12*, 4105. [CrossRef]
12. Yang, S.; Yu, Q. The role of fluid-rock interactions in permeability behavior of shale with different pore fluids. *Int. J. Rock Mech. Min. Sci.* **2022**, *150*, 105023. [CrossRef]
13. Chen, Y.; Cao, P.; Chen, R.; Teng, Y. Effect of water–rock interaction on the morphology of a rock surface. *Int. J. Rock Mech. Min. Sci.* **2010**, *47*, 816–822. [CrossRef]
14. Poulsen, B.; Shen, B.; Williams, D.; Huddlestone-Holmes, C.; Erarslan, N.; Qin, J. Strength reduction on saturation of coal and coal measures rocks with implications for coal pillar strength. *Int. J. Rock Mech. Min. Sci.* **2014**, *71*, 41–52. [CrossRef]
15. Perera, M.; Ranjith, P.; Peter, M. Effects of saturation medium and pressure on strength parameters of Latrobe Valley brown coal: Carbon dioxide, water and nitrogen saturations. *Energy* **2011**, *36*, 6941–6947. [CrossRef]
16. Vishal, V.; Ranjith, P.; Singh, T. An experimental investigation on behaviour of coal under fluid saturation, using acoustic emission. *J. Nat. Gas Sci. Eng.* **2015**, *22*, 428–436. [CrossRef]
17. Wang, W.; Wang, H.; Li, D.; Li, H.; Liu, Z. Strength and Failure Characteristics of Natural and Water-Saturated Coal Specimens under Static and Dynamic Loads. *Shock Vib.* **2018**, *2018*, 3526121. [CrossRef]

18. Yao, Q.; Chen, T.; Ju, M.; Liang, S.; Liu, Y.; Li, X. Effects of Water Intrusion on Mechanical Properties of and Crack Propagation in Coal. *Rock Mech. Rock Eng.* **2016**, *49*, 4699–4709. [CrossRef]
19. Qin, H.; Huang, G.; Wang, W. Experimental study of acoustic emission characteristics of coal samples with different moisture contents in process of compression deformation and failure. *Chin. J. Rock Mech. Eng.* **2012**, *31*, 1115–1120.
20. Feng, G.; Wen, X.; Guo, J.; Wang, P.; Qian, R.; Yan, Y.; Hao, C. Study on influence of moisture content on coal sample AE properties and fragment distribution characteristics. *J. Cent. South Univ.* **2021**, *52*, 2910–2918. [CrossRef]
21. Yao, Q.; Wang, W.; Li, X.; Tang, C.; Xu, Q.; Yu, L. Study of mechanical properties and acoustic emission characteristics of coal measures under water-rock interaction. *J. China Univ. Min. Technol.* **2021**, *50*, 558–569.
22. Zhang, M.; Nie, R. Experimental Investigation on the Influence of Water Content on the Mechanical Properties of Coal under Conventional Triaxial Compression. *Shock Vib.* **2020**, *2020*, 8872438. [CrossRef]
23. Liu, F.; Han, Y. Mechanical Behavior and Impact Resistance Tendency of Coal Mass with Different Water Content. *Geofluids* **2022**, *2022*, 9128287. [CrossRef]
24. Wang, C.; Gao, Y.; Guo, C.; Wei, K. Experimental study on the influence of moisture content on soft coal strength characteristics. *Int. J. Min. Miner. Eng.* **2021**, *12*, 163–180. [CrossRef]
25. Wang, L.; Zhu, C.; Yin, Z.; Hou, J. Research on soft coal mechanics characteristic test for moisture content effect. *J. Min. Saf. Eng.* **2016**, *33*, 1145–1151. [CrossRef]
26. Zhu, C.; Li, C.; Yin, Z.; Hou, J. Experimental study of soft coal mechanics characteristics with different moistures and clay contents. *Chin. J. Rock Mech. Eng.* **2017**, *36*, 3258–3265. [CrossRef]
27. Krajcinovic, D.; Silva, M.A.G. Statistical aspects of the continuous damage theory. *Int. J. Solids Struct.* **1982**, *18*, 551–562. [CrossRef]
28. Hu, X.; Hong, B.N.; Meng, Y.M. Statistical damage model of red sandstone with effect of water ratio considered. *J. China Univ. Min. Technol.* **2007**, *36*, 609–613. [CrossRef]
29. Zhou, Z.; Cai, X.; Cao, W.; Li, X.; Xiong, C. Influence of Water Content on Mechanical Properties of Rock in Both Saturation and Drying Processes. *Rock Mech. Rock Eng.* **2016**, *49*, 3009–3025. [CrossRef]
30. Bian, K.; Liu, J.; Zhang, W.; Zheng, X.; Ni, S.; Liu, Z. Mechanical Behavior and Damage Constitutive Model of Rock Subjected to Water-Weakening Effect and Uniaxial Loading. *Rock Mech. Rock Eng.* **2019**, *52*, 97–106. [CrossRef]
31. Liu, D.; He, M.; Cai, M. A damage model for modeling the complete stress–strain relations of brittle rocks under uniaxial compression. *Int. J. Damage Mech.* **2018**, *27*, 1000–1019. [CrossRef]
32. Wang, K.; Jiang, Y.; Xu, C. Mechanical properties and statistical damage model of coal with different moisture contents under uniaxial compression. *Chin. J. Rock Mech. Eng.* **2018**, *37*, 1017–1026. [CrossRef]
33. Chen, Y.; Cui, H.; Pu, H.; Wu, P.; Chen, L.; Zhang, K. Study on Mechanical Properties and Cracking Mode of Coal Samples under Compression–Shear Coupled Load Considering the Effect of Loading Rate. *Appl. Sci.* **2020**, *10*, 7082. [CrossRef]
34. Qi, Q.; Peng, Y.; Li, H.; Li, J.; Wang, Y.; Li, C. Study of bursting liability of coal and rock. *Chin. J. Rock Mech. Eng.* **2011**, *30*, 2736–2742.
35. Li, Y.; Jiang, Y.; Zhang, B.; Song, H.; Dong, W.; Wang, P. Investigation on the pore characteristics of coal specimens with bursting proneness. *Sci. Rep.* **2019**, *9*, 16518. [CrossRef]
36. Qiang, L. Response Analysis of Deformation of Roadway Surrounding Rock Seepage of Water Coupled System under the Condition That Coal Seam Is Main Aquifer. Ph.D. Thesis, China University of Mining & Technology, Xuzhou, China, 2015.
37. Li, S.C.; Li, Q.; Miao, X.X.; Chen, Z.Q. Experimental study on permeability properties of stratum medium of Xiaojihan coal mine and genetic mechanism of the coal seam becoming a main aquifer. *J. China Coal Soc.* **2017**, *42*, 353–359. [CrossRef]
38. You, Q.; You, M. Statistical damage constitutive models of rock and their comparative analysis. *J. Lanzhou Univ. Technol.* **2011**, *37*, 119–123.
39. Wong, T.-F.; Wong, R.H.C.; Chau, K.T.; Tang, C.A. Microcrack statistics, Weibull distribution and micromechanical modeling of compressive failure in rock. *Mech. Mater.* **2006**, *38*, 664–681. [CrossRef]
40. Lemaitre, J. How to use damage mechanics. *Nucl. Eng. Des.* **1984**, *80*, 233–245. [CrossRef]
41. Zhang, Q.; Yang, G.; Ren, J. New study of damage variable and constitutive equation of rock. *Chin. J. Rock Mech. Eng.* **2003**, *22*, 30–34.
42. Lu, Z.D. Experimental and Theoretical Analysis on Mechanical Properties of Fractured Rock under Water-Rock Interaction. Ph.D. Thesis, Chinese Academy of Sciences, Wuhan, China, 2010.